



AN EXPERIMENTAL STUDY OF DRAG ON A SINGLE TUBE AND ON A TUBE IN AN ARRAY UNDER TWO-PHASE CROSS FLOW

Y. JOO and V. K. DHIR

Mechanical, Aerospace and Nuclear Engineering Department, School of Engineering and Applied Science, University of California, Los Angeles, Los Angeles, CA 90024, U.S.A.

(Received 21 September 1993; in revised form 26 April 1994)

Abstract—In this work, the drag coefficient and the void fraction around a tube subjected to two-phase cross flow were studied for a single tube and for a tube placed in an array. The drag coefficients were determined by measuring the pressure distribution around the perimeter of the tube. Single tube drag data were taken when the tube was held both rigidly and flexibly. The test tube was made of acrylic and was 2.2 cm in diameter and 20 cm in length. In the experiments, liquid Reynolds number ranged from 430 to 21,900 for the single tube and liquid gap Reynolds number ranged from 32,900 and 61,600 for the tube placed in a triangular array. Free stream void fraction was varied from 0 to 0.4. At low Reynolds numbers, the ratio of two-phase to single-phase drag coefficient is found to be a strong function of $\epsilon Gr/Re^2$. However, at high Reynolds numbers only void fraction is the important parameter. Empirical correlations have been developed for the ratio of two-phase drag on a single tube and on a tube placed in an array.

Key Words: two-phase flow, cross flow, drag coefficient, void fraction, tube array

1. INTRODUCTION

Two-phase cross flow over tubes occurs in many shell-and-tube heat exchangers, steam generators, condensers and other equipment utilized in power and process industries. However, only a few studies of the two-phase drag experienced by such tubes have been reported in the literature. A knowledge of the drag coefficient for a tube, the void fraction distribution and bubble behavior near a tube subjected to two-phase cross flow is essential for development of mechanistic understanding of fluidelastic instability of tubes subjected to two-phase cross flow.

Yokosawa *et al.* (1986) measured the drag on a single tube under two-phase cross flow in the Reynolds number range of 4000–300,000 and for low void fractions (0–0.1). In the experiments cylinders of 10, 20, 30 or 40 mm in diameter and 58 mm in length were used. The cylinders were made of brass and were held rigidly or flexibly. For rigidly mounted tubes, they determined the drag force from pressure distributions on the tubes. For flexibly mounted tubes, cantilever beam supports which were instrumented with strain gages were used. The drag coefficients from both methods were almost similar. They found that the drag coefficient decreased with increasing void fraction for two-phase Reynolds numbers sufficiently below the single-phase critical Reynolds number. But, for Reynolds numbers above the critical value, the drag coefficient was found to gradually increase with increasing void fraction, although it remained significantly less than the value for subcritical, single-phase flow. However, the void fraction was not increased sufficiently to observe an increase in drag coefficient above that for single-phase flow.

In the first part of the same study (Inoue *et al.* 1986), the void fraction distribution around the tube was measured with an electrical impedance probe inserted in the flow in the Reynolds number range of 5000–80,000. They found that high void fraction regions, with the local void fraction about 3–4 times higher than the free stream value, were produced near the separation point. As the mean velocity in the main flow increased, this peak void fraction also increased and the location of the peak void fraction came closer to the cylinder. However, they did not measure void fractions upstream of the tube. From photographs, they noted liquid-rich layers in the front and in the rear of the tube. As the mean velocity increased, the liquid layer became thicker in the front of the tube and thinner in the rear of the tube.

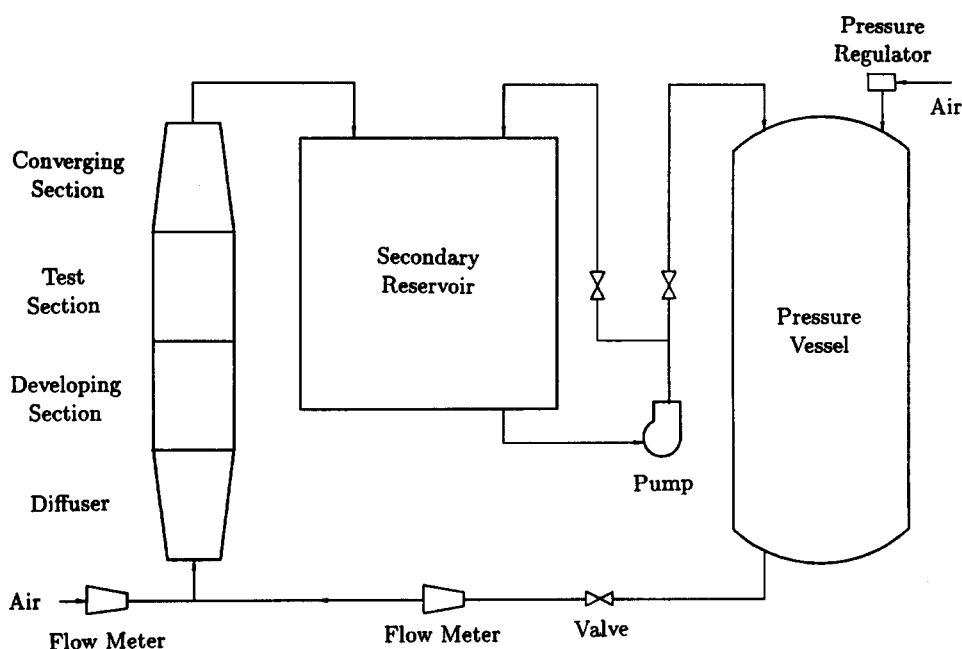


Figure 1. A schematic diagram of the flow loop.

Pettigrew *et al.* (1988) studied vibrations of a tube in a square array, in a normal triangular array and in a parallel triangular array configuration with pitch to diameter ratios of 1.32 and 1.47. Stainless steel tubes of 600 mm length, 13 mm diameter and 1.07 mm wall thickness were used. By taking photographs of the flow at the end of the bundle, they observed relatively stagnant zones of mostly liquid immediately upstream and downstream of each tube. These zones appeared to be symmetrical about the equator of the tube. A two-phase mixture occupied the region around these zones.

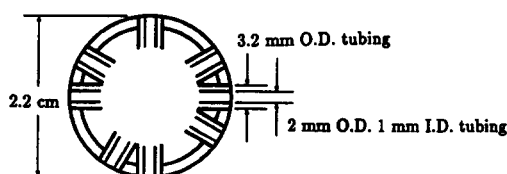
At present no quantitative correlation for two-phase drag on cylinders subjected to two-phase cross flow is available in the literature. The purpose of the present work is to develop such a correlation. Void fractions around a single tube and around a tube in an array will also be measured to understand the fluid behavior in two-phase cross flow.

2. EXPERIMENTAL APPARATUS AND PROCEDURE

2.1. Two-phase flow loop

A schematic diagram of the flow loop for air-water two-phase flow is shown in figure 1. It is primarily formed with an 11.4 cm diameter PVC pipe. A 1000 gpm ($0.063 \text{ m}^3/\text{s}$) capacity pump or a 300 gpm ($0.019 \text{ m}^3/\text{s}$) capacity pump supplies water from the secondary reservoir to the pressure vessel. The capacities of the secondary reservoir and the pressure vessel are 3.9 and 2.5 m^3 , respectively. A by-pass line is connected from the main pipe to the secondary reservoir. A butterfly valve is installed in the main pipe and a gate valve is installed in the by-pass line. Water flow rate from the pump to the pressure vessel is controlled with a combination of these valves. Free surface of water in the pressure vessel is pressurized with utility air. A pressure regulator keeps the air pressure constant. This in turn allows a constant flow rate to be maintained from the vessel to the remaining sections of the loop. The pressure in the pressure vessel is regulated from 0.14 MPa at low flow rates (about $0.012 \text{ m}^3/\text{s}$) to 0.19 MPa at high flow rates (about $0.02 \text{ m}^3/\text{s}$). Water exits the pressure vessel through a globe valve and passes through a turbine flow meter. During the experiments, water flow rate is controlled with this globe valve.

The liquid stream then turns upward to flow vertically through the test section assembly. When two-phase flow is desired, utility air is introduced through one or more injection holes placed upstream of the test section. Air entering an injection hole passes through a flow meter with a pressure gage. A correction to the measured air flow rate is made for the pressure being different



Single tube



Tube in an array

Figure 2. Pressure tap distribution.

than that at which the flow meter was calibrated. Air bubbles are broken up by a series of wire meshes which homogenize the mixture before it enters the diffuser. After expansion in the diffuser, which expands at an angle of 7 degrees, the flow is stabilized in the flow developing section. It then passes through the test section, in which the test tube is installed. The flow-developing section and the test section have the same dimensions: 30 cm high with a 12.5×20 cm cross section. The flow exits through a converging section which has dimensions identical to those of the diffuser. The test section assembly—diffuser, flow-developing section, test section and converging section—are made with transparent half inch thick Plexiglas plates. The flow exiting the test section is released to the secondary reservoir, where air is allowed to escape. The uncertainty in air and water flow rate are calculated to be ± 2 and $\pm 0.4\%$, respectively.

2.2. Drag coefficient for a rigidly and flexibly mounted single tube

The acrylic test tube of 2.2 cm in diameter and 20 cm in length is mounted horizontally in the test section. The tube is instrumented with pressure taps to measure the pressure distribution and in turn the drag coefficient. The taps are located at angles of $0, -30, 60, \pm 90, \pm 120$ and 180 degrees from the lower stagnation point. Each tap is 3.2 mm in diameter. A 3.2 mm outer diameter tygon tubing is inserted inside each tap. Another 1 mm i.d., 2 mm o.d. Teflon tubing is inserted in the tygon tube to avoid air bubbles from entering the tube during experiments. Outside the test section, the tubing is again expanded through a reducing union to a 3.2 mm i.d., 6.4 mm o.d. polyethylene tubing. Taps at the lower stagnation point are connected to each of the remaining taps through a manometer. Each line has a valve for the expulsion of any bubbles in the line. The orientation of the pressure taps is shown in figure 2.

The drag coefficient (C_D) is calculated from the pressure distribution by using the following equation:

$$C_D = \frac{gD}{V_L^2} \left(\frac{\pi\epsilon}{2} + \int_0^{2\pi} C_1 \frac{\Delta}{D} \cos \theta \, d\theta \right) \quad [1]$$

and the lift coefficient (C_L) is calculated by using the equation:

$$C_L = -\frac{gD}{V_L^2} \int_0^{2\pi} C_1 \frac{\Delta}{D} \sin \theta \, d\theta \quad [2]$$

where D is a tube diameter, V_L is the superficial liquid velocity at free stream, g is the gravitational acceleration, ϵ is a free stream void fraction, Δ is the difference in hydrostatic head in millimeter of water from that at the lower stagnation point, θ is the angular position measured from the lower stagnation point of the tube and C_1 is a constant which depends upon the angle that the

manometers are inclined from the horizontal. The uncertainty in the measurement of the drag and lift coefficients is calculated to be less than $\pm 10\%$. The drag coefficient was measured by varying the liquid Reynolds number (Re_L) from 430 to 21,900 based on superficial liquid velocity.

The same test section was used for flexibly mounted tubes as for rigidly mounted tubes. The acrylic test tube of 2.2 cm in diameter and 25 cm in length extends through holes in the test section wall. The tube was flexibly supported with two cantilever beams which were held at the outside of the test section wall. The holes in the test section wall are large enough to give the test tube sufficient room to vibrate. Easily removable caps cover the cantilever beams and holes to prevent leaking. The test tube can vibrate in only one direction—normal to the cantilever beams.

The cantilever beams which support the test tube are made from spring steel plates. For the single tube experiments, the cantilever beam thickness was 0.45 mm, the width was 6.5 mm and the length was 53.5 mm. The tube mass was 0.068 kg, and the natural frequency in water was 6.7 Hz.

The drag coefficient on a flexibly mounted tube was measured in two ways: from the pressure distribution around the tube and from the strain gages signals. The pressure distribution was measured in exactly the same manner as for a 2.2 cm rigidly mounted tube. Strain gages were placed on the upper and lower surface of each cantilever beam. The strain gages were installed at 6 mm from the beam supporting palates. The data from the strain gages were read from the strain gage input module in the data acquisition system. The mean displacements of the test tube were calculated with a personal computer which was connected to the data acquisition system. Drag force on the tube was determined from this mean value of displacement of the tube.

When the strain gage were used to calculate the drag coefficient, the test section was filled with water and a certain time period was allowed for the water to become calm. The strain gage output was measured in still water. Since the strain gage module could not be set at zero for the signal in still water, this value was used to compensate the measured response during flow. Thereafter, the pump was started and the strain gage signal was measured. The uncertainty due to strain gage reading and flow rate is calculated to be $\pm 15\%$.

Strain gages were calibrated prior to an experiment. Known forces were applied to the test tube, and strain gage signals were recorded at each time. A linear relationship between applied force–strain gage signal was obtained. From these data, each strain gage signal was converted to the force acting on the tube.

2.3. Drag coefficient for the rigid tube in an array

The experiments were performed not only for a single tube but also for a tube array. For the tube array, the dummy tubes of the same size as the test tubes are arranged in a triangular grid with a pitch to diameter ratio of 1.4 (figure 3). Half tubes are installed on each side of the tube

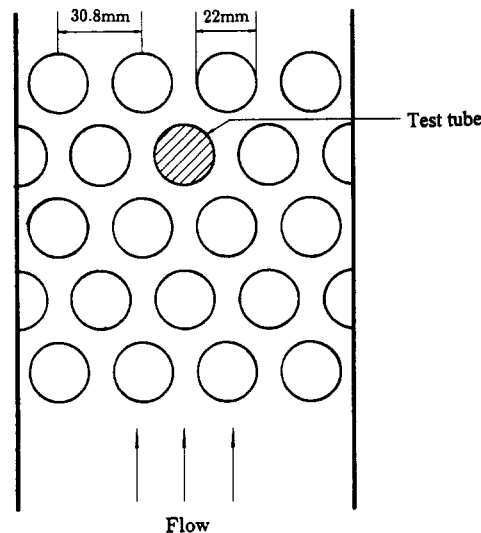


Figure 3. A normal triangular tube array.

bundle to minimize the wall effect. The bundle contains five rows of tubes, and the test tube is located in the middle of the fourth row. The test tube in an array has pressure taps at angles of 0, ± 30 , ± 60 , ± 120 , ± 150 and 180 degrees. Data for a flexibly mounted tube in an array were not taken because the displacement of a tube in an array was found to affect the measured drag.

For a triangular array, the superficial liquid gap velocity is calculated using the equation

$$V_r = \frac{P}{P - D} V_L \quad [3]$$

where V_r is the superficial liquid gap velocity and V_L is the superficial liquid velocity at free stream. P and D are pitch and diameter of the tubes. In the experiments, the liquid gap Reynolds number (Re_r) based on superficial liquid gap velocity was varied from 32,900 to 61,600 while the liquid Reynolds number based on free stream velocity was varied from 9400 to 17,600.

2.4. Void fraction measurements

The Plexiglas test section allowed the use of a gamma densitometer to measure the time-averaged void fraction at various positions. The gamma densitometer consists of a cesium-137 source and an NaI detector. The gamma beam created by the source is collimated by passing through a small opening in the source's lead housing. It then passes through the test section, and is again collimated by passing it through a small opening in the detector's lead housing. Gamma rays are absorbed in the detector, producing electronic pulses. A 1024-channel analyzer sorts the pulses into different channels, depending on the energy of each pulse, and stores them. The number of pulses is plotted versus channel number, and the integral under the curve (I) is evaluated within the region of interest amongst all the channels. The value of I is recorded and used to calculate the void fraction using the following equation:

$$\epsilon = \frac{\ln(I/I_L)}{\ln(I_G/I_L)} \quad [4]$$

where I_L and I_G are the integrals under the curve for water and air, respectively. The uncertainty of void fraction measurement with the gamma densitometer itself is $\pm 3\%$. However, when the void fraction is measured very near the tube, the uncertainty in the position also becomes important. For the measurement of void fraction in a tube array, the maximum value of total uncertainty is calculated to be $\pm 20\%$. This uncertainty occurs very near the tube wall. The uncertainty of data away from the tube is much less.

The free stream void fractions in the test section were measured upstream of a tube bundle. From this data, an empirical correlation was obtained as

$$19.65(1 - \epsilon)^3 \left(\frac{V_G(1 - \epsilon)}{\epsilon} - V_L \right)^2 - 1 = 0 \quad [5]$$

where V_G is the superficial gas velocity. The velocity is measured in meters per second. The free stream void fraction in a given experiment was calculated by using this correlation.

3. RESULTS

3.1. Drag coefficient on a single tube

The pressure distribution around the perimeter of the tube was measured using manometers. Figure 4 shows one of the typical pressure distribution profiles around a tube at a liquid Reynolds number of 8200 and a free stream void fraction of 0.25. The pressure plotted is the difference in pressure from that at the lower stagnation point (the upstream stagnation point). The pressure on the surface of the tube is maximum at the lower stagnation point and decreases along the tube perimeter. The pressure is minimum at 90 degrees, where the flow velocity is expected to be maximum. After passing the 90 degree point, pressure increases again as flow expands. However, the pressure at the 180 degree point does not return to its value at 0 degrees because of a wake behind the tube. The pressure distribution is symmetrical about the vertical axis passing through the center of the tube and parallel to the flow.

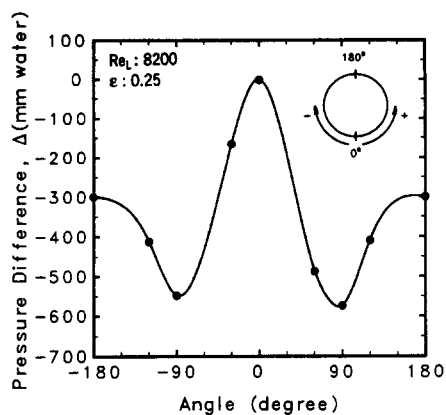


Figure 4. Pressure distribution around a single tube.

The drag coefficient was obtained by taking the integral of the pressure difference multiplied by the cosine of the angle around the tube as given in [1]. In figure 5, the drag coefficients for a single rigidly and flexibly mounted tube are plotted as a function of free stream void fraction for various liquid Reynolds numbers. The open symbols represent data for the rigidly mounted tube whereas the solid symbols are for data obtained on a flexibly mounted tube. The data obtained on rigidly and flexibly mounted tubes nearly overlap. At low liquid Reynolds numbers addition of gas dramatically increases the drag coefficient. However, at high liquid Reynolds numbers the effect of the presence of a second phase on drag diminishes. At a liquid Reynolds number of 430, the drag coefficient for a free stream void fraction of 0.36 is 717, which is about 600 times the value for single-phase flow. On the other hand, for a liquid Reynolds number of 8200 and a free stream void fraction of 0.36, the drag coefficient is 4.3. This value is only about four times the single-phase value. The large increase in drag coefficient at small liquid Reynolds numbers is probably caused by a relatively large difference in velocity that exists between gas and liquid. On a macroscopic level this difference manifests in the form of an increased effective velocity of the liquid.

Interestingly at a liquid Reynolds number of 21,900, the drag coefficient for a free stream void fraction of 0.046 is only 0.81, which is less than (about 0.6 times) the single-phase value of 1.3. This behavior is similar to that observed by Inoue *et al.* (1986). With further increase in the free stream void fraction, the drag coefficient is again found to exceed the value for single-phase flow.

The lift coefficient was obtained by taking the integral of the pressure difference multiplied by the sine of the angle around the tube ([2]), even though it was expected to be zero from theory. The magnitude of the lift coefficient is indicative of the extent of uncertainty in the drag data. The

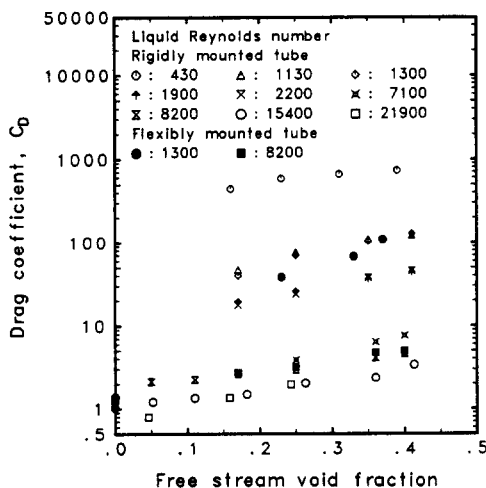


Figure 5. Drag coefficient over a single tube.

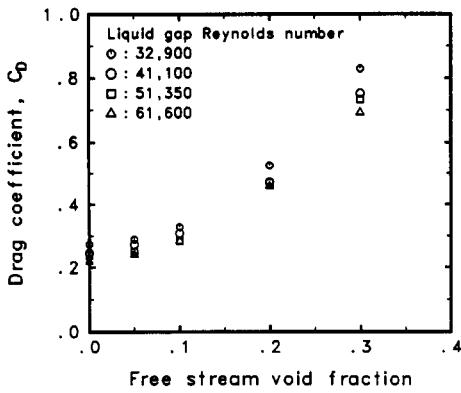


Figure 6. Drag coefficient over a tube in an array.

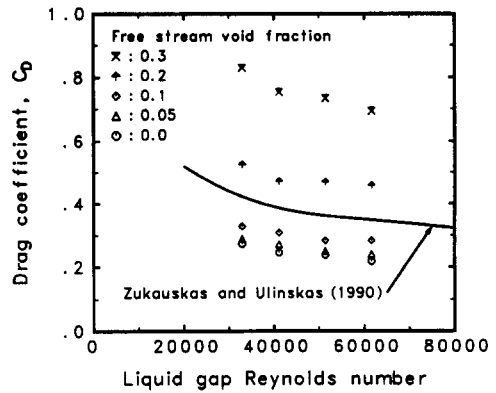


Figure 7. Drag coefficient over a tube in an array.

lift coefficient was found to be at least an order of magnitude smaller than the drag coefficient at high velocities, while it was at least two orders of magnitude smaller than the drag coefficient at lower velocities.

3.2. Drag coefficient for a tube in an array

The pressure distributions around the perimeter of the tube in a triangular array were also measured. In figures 6 and 7, the drag coefficients obtained from these pressure distribution data are plotted as a function of free stream void fraction and liquid gap Reynolds number. The drag coefficient increases as the free stream void fraction increases but decreases as the liquid gap Reynolds number increases. The prediction from the curve drawn through the data of Zukauskas & Ulinskas (1990), which was obtained for single-phase flow across a tube in a triangular array, are also plotted in figure 7. Present data for single-phase flow are found to be about 35% lower than the data of Zukauskas & Ulinskas.

3.3. Void fraction profile

Figure 8 (a) shows vertical void fraction profile near a single tube. For the plotted data the free stream void fraction was 0.25, and the liquid Reynolds number was 430. Approaching the tube from below, the void fraction increases gradually until just below the lower stagnation point. A decrease in void fraction is detected immediately downstream of the cylinder. Thereafter, the void fraction gradually returns to the free stream value. For the same flow conditions, the circumferential void fraction profile at various radii are plotted in figure 8 (b). The gas-rich region on the upstream portion and a liquid-rich region on the downstream portion can be seen clearly in the figures. It should also be noted that a minimum distance of about 40–45 mm from the tube center is needed for the void fractions both upstream and downstream of the tube to approach the free stream undisturbed value.

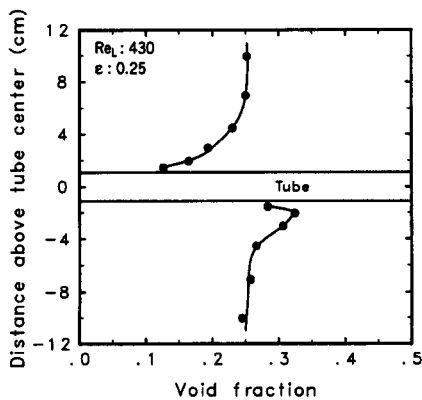


Figure 8. (a) Vertical void fraction profile near a single tube at low Reynolds number.

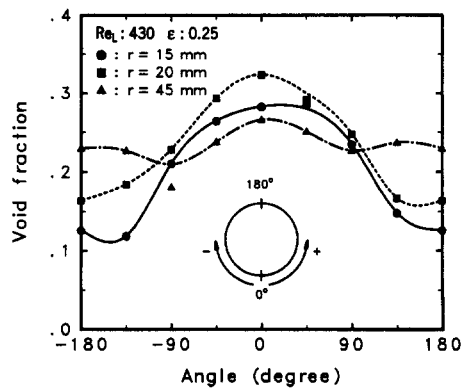


Figure 8. (b) Circumferential void fraction profile around a single tube at low Reynolds number.

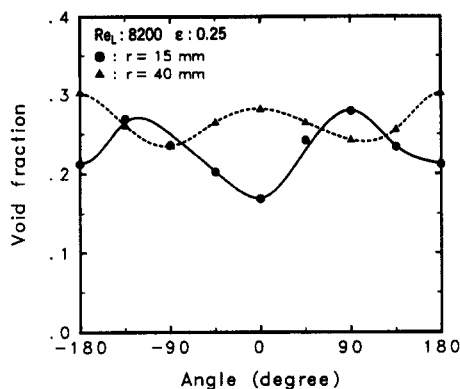
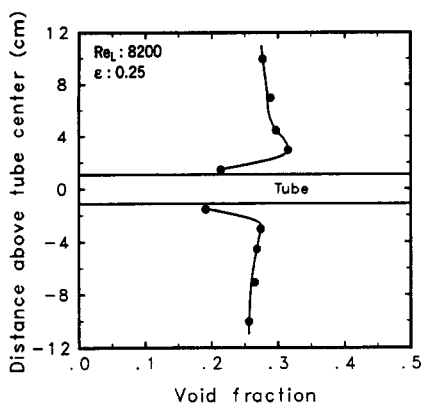


Figure 9. (a) Vertical void fraction profile near a single tube at high Reynolds number.

Figure 9. (b) Circumferential void fraction profile around a single tube at high Reynolds number.

Figures 9 (a) and (b) show the vertical and the circumferential void fraction profiles at a liquid Reynolds number of 8200, and a free stream void fraction of 0.25. The void fraction is minimum very near the lower stagnation point (0 degrees), and then increases along the circumference. It attains a maximum value between 90 and 135 degrees, and then decreases up to the downstream stagnation point. Thus liquid-rich regions occupy both upstream and downstream stagnation point regions.

At low liquid velocities the boundary layer near the forward stagnation point is relatively thicker and bubbles accumulate there. With increase in velocity the boundary layer thins and bubbles simply follow the streamlines and only a small accumulation of bubbles occurs near the forward stagnation point. In the region downstream of the 90 degrees, the bubbles again begin to accumulate as the fluid starts to slow down and pressure starts to recover. However, only a few of the bubbles are entrained in the wake behind the cylinder for all flows and, as a result, a liquid-rich region is observed near the downstream stagnation point. The latter observation is consistent with the result of Inoue *et al.* (1986). However, Inoue *et al.* did not observe a gas-rich region near the forward stagnation point; the reason being that liquid Reynolds numbers in their experiments were always higher than 5000.

A circumferential void fraction profile around a tube in a normal triangular array is plotted in figure 10. The liquid gap Reynolds number is 41,000 and the free stream void fraction is 0.15. The void fractions at two different radii were measured. For the position near the tube (radius of 13.5 mm), void fraction is minimum at the lower stagnation point (0 degrees), and then increases along the circumference. It attains a maximum value at an angle of 150 degrees, and then decreases at 180 degrees. This profile has a very similar shape to the case of the single tube at a radius of 15 mm in figure 9 (b). The void fraction profile at 15.4 mm radius has two peaks of about the same magnitude at 30 and 150 degrees. This is because 30 and 150 degree points on a radius of 15.4 mm

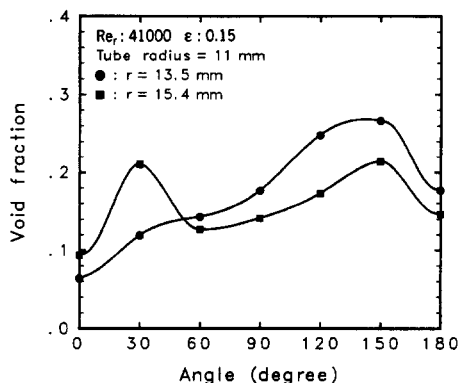


Figure 10. Void fraction distribution in a triangular tube array ($P/D = 1.4$).

are the midpoints between two adjacent tubes and represent the smallest flow area. From their work Pettigrew *et al.* (1988) noted that the flow pattern was symmetrical about the tube equator. However, from the present data it can be seen that upstream and downstream void fraction profiles in the vicinity of the tube are asymmetrical.

4. DISCUSSION

4.1. Void fraction profiles

Near a single tube the void fraction is seen to depend both on the radius and the angular position. At low liquid Reynolds numbers, accumulation of gas in the front of the tube is observed while a deficiency of void exists near the downstream stagnation point. At high liquid Reynolds numbers, void deficient regions are observed at both upstream and downstream stagnation points. For a tube in an array, the void fraction profiles very near the tube are asymmetric with respect to the equator. However, the asymmetry tends to diminish the radial distance away from the tube. Both gas and liquid superficial velocities in the gap between the tubes increase. Using [5], it is found that void fraction in the tube bundle should be about 30% larger than that in the free stream. Void profiles such as those shown in figure 10 indeed show an increase in the average void fraction in the flow passage.

4.2. Correlation of two-phase drag coefficient

Pressure distributions around a single tube showed that for liquid Reynolds numbers less than about 10,000, addition of gas in the fluid resulted in a larger and rapid decrease of pressure in the frontal portion of the tube. In the downstream direction of the tube, however, the pressure did not recover to its single-phase value. Although it is difficult to separate the pressure drop due to acceleration of the flow and that due to viscous dissipation, it appears that presence of a bubble in the flow tends to squeeze the flow lines in the frontal portion whereas in the section downstream of the equator, the bubble tends to inhibit the expansion of the flow lines. The viscous dissipation increases because of the relative velocity that exists between gas and liquid. The interfacial area between gas and liquid also increases with increase in gas flow rate or void fraction. The net effect being that the drag force or drag coefficient on the tube increases with increase of void fraction.

For liquid Reynolds numbers of 15,400 and 21,900 a reduction in the drag coefficient was observed with the addition of a small amount of gas. The pressure distribution data for these liquid Reynolds numbers showed, on the frontal region of the tube, a behavior similar to that observed for low liquid Reynolds numbers. However, a small amount of gas in the flow was found to have little or no effect on the wake region. At higher free stream void fractions, the behavior was similar to that observed at low liquid Reynolds numbers. Pressure distribution around a tube in an array showed a behavior similar to that of a single tube.

The ratios of two-phase to single-phase drag coefficients for a single tube and for a tube in an array are plotted in figure 11, as a function of Reynolds number. The plotted data are for void fractions in the range 0.25–0.4. For a single tube, liquid Reynolds number and free stream void

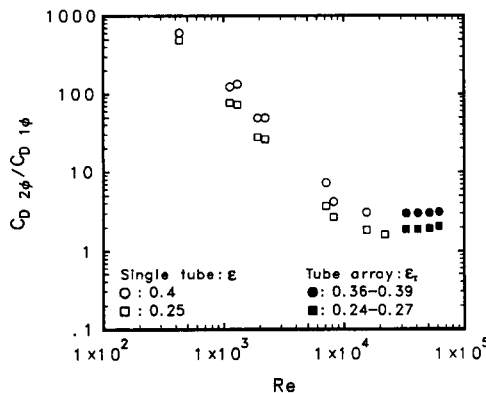


Figure 11. The ratio of two-phase to single-phase drag coefficient for a single tube and for a tube array.

fraction are used whereas for a tube in an array liquid gap, Reynolds number and average gap void fraction (ϵ_r) are used. The average gap void fractions were obtained from [5] by substituting superficial liquid and gas gap velocities instead of free stream superficial liquid and gas velocities. It is seen that the ratio of two-phase to single-phase drag coefficients decreases with Reynolds numbers and appears to reach an asymptotic value after a Reynolds number of about 20,000. Consistent with the data at lower Reynolds numbers, the asymptotic value of the ratio is higher at higher void fractions. The clear distinction between data for a tube in an array and a single tube is not observed as the array data appear to be simply an extension of the single tube data.

For single-phase flow, the Reynolds number is a key correlation parameter for the drag coefficient. Density difference between gas and liquid leads to a buoyancy force which manifests itself as a velocity difference between gas and liquid. The velocity difference between the two phases leads to additional viscous dissipation. As such the Grashof number is considered to be an important parameter. The Grashof number is defined as

$$Gr = \frac{(\rho_L - \rho_G)gD^3}{\rho_L \nu_L^2} \tag{6}$$

where ρ_L and ρ_G are densities of water and air, respectively, and ν_L is the kinematic viscosity of water. Although in the present experiment Gr was not varied, there is ample precedence in the literature (see, for example, Drucker *et al.* 1984 and Kianjah & Dhir 1989) to use this group to describe the effect on drag and heat transfer of addition of a discontinuous phase in a continuous phase. The presence of voids in the fluid not only influences the viscous dissipation but also affects the flow lines as was discussed earlier. Thus the key dimensionless parameters considered to be important in correlating the two-phase drag data are: ϵ , Gr and Re . In figure 12, the data for the ratio of two-phase to single-phase drag coefficients obtained on a single tube and on a tube in an array are plotted as a function of $\epsilon Gr/Re^2$. All of the data are correlated to within $\pm 30\%$ as

$$\frac{C_{D2\phi}}{C_{D1\phi}} = 1 + 3\left(\frac{\epsilon Gr}{Re^2}\right) + 12\epsilon^2 \quad \text{for} \quad 2 \times 10^{-3} < \frac{\epsilon Gr}{Re^2} < 4 \times 10^2 \quad \text{and} \quad \epsilon < 0.4 \tag{7}$$

where Re and ϵ are the liquid Reynolds number (Re_L) and the free stream void fraction for a single tube and the liquid gap Reynolds number (Re_r) and the average gap void fraction (ϵ_r) for a tube in an array. As Reynolds number becomes larger or liquid inertia increases, the effect of void on viscous dissipation in the flow diminishes and eventually the ratio of two-phase to single-phase becomes nearly independent of $\epsilon Gr/Re^2$. However, the effect of void fraction in altering the flow field continues to persist. For single-phase drag coefficients in a single tube, Roshko's data (1961) were used because single-phase data taken in the present work were found to compare well with the data of Roshko. Single-phase drag coefficients on a tube in a bundle were correlated as

$$C_{D1\phi} = \frac{5.5}{Re_r^{0.3}} \tag{8}$$

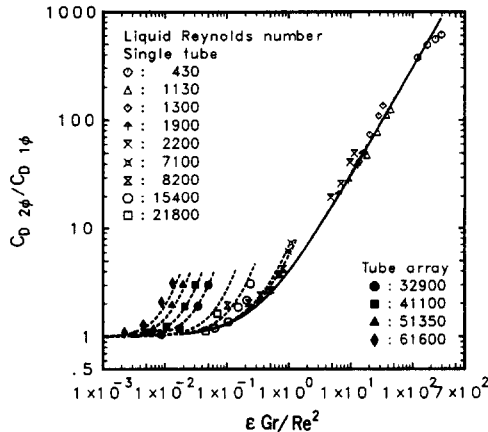


Figure 12. Empirical correlation of the ratio of two-phase to single-phase drag coefficient (---) ([7]).

It is interesting to note that Drucker *et al.* correlated their ratio of bubbly flow to single-phase heat transfer data with $(\epsilon Gr/Re^2)^{0.5}$. Their data were in the range $10^{-1} < \epsilon Gr/Re^2 < 10$ with $\epsilon < 0.15$. It is possible that they did not recognize the existence of the ϵ^2 term because its contribution to their data was relatively non significant.

5. CONCLUSIONS

(1) For two-phase cross flow over tubes, deficiency of voids in the region near the downstream stagnation point is observed for all Reynolds numbers. At low Reynolds numbers a gas-rich region is observed ahead of the forward stagnation point. However, this trend appears to reverse as Reynolds numbers become large.

(2) Void profiles for a single tube and for a tube in an array are asymmetrical with respect to the equator.

(3) Two-phase drag coefficients are much higher than those for single-phase flow. The ratio of two-phase to single-phase drag coefficients decreases as Reynolds number becomes large or inertia of the base flow increases.

(4) The ratios of two-phase to single-phase drag coefficient data have been correlated with ϵ^2 and $\epsilon Gr/Re^2$.

Acknowledgement—This work received support from the United States Department of Energy under Contract No. DE-FG07-89ER-12902.

REFERENCES

- DRUCKER M. I., DHIR, V. K. & DUFFEY, R. B. 1984 Two-phase heat transfer for flow in tubes and over rod bundles with blockages. *Trans. ASME, J. Heat Transfer* **106**, 856–864.
- INOUE, A., KOZAWA, Y., YOKOSAWA, M. & AOKI, S. 1986 Studies on two-phase cross flow. Part I: flow characteristics around a cylinder. *Int. J. Multiphase Flow* **12**, 149–167.
- KIANJAH H. & DHIR, V. K. 1989 Experimental and analytical investigation of dispersed flow heat transfer. *Exp. Therm. Fluid Sci.* **2**, 410–424.
- PETTIGREW, M. J., TROMP, J. H., TAYLOR, C. E., & KIM, B. S. 1988 Vibration of tube bundles in two-phase cross-flow: Part 2—fluidelastic instability. *ASME Int. Symp. on Flow-induced Vibrations and Noise, Winter Annual Meeting*, Vol. 3, pp. 159–179, Chicago, IL.
- ROSHKO, A. 1961 Experiments on the flow past a circular cylinder at very high Reynolds number. *J. Fluid Mech.* **10**, 345–356.
- YOKOSAWA M., KOZAWA Y., INOUE, A. & AOKI, S. 1986 Studies on two-phase cross flow. Part II: transition Reynolds number and drag coefficient. *Int. J. Multiphase Flow* **12**, 169–184.
- ZUKAUSKAS, A. & ULINSKAS, R. 1990 Banks of plain and finned tubes. In *Hemisphere Handbook of Heat Exchanger Design* (Edited by HEWITT, G. F.), Chap. 2.2.4. Hemisphere, New York.